Epitaxial graphene on 3C-SiC(111) pseudosubstrate: Structural and electronic properties

A. Ouerghi,[1] M. Marangolo,[2] R. Belkhou,[3] S. El Moussaoui,[3] M. G. Silly,[3] M. Eddrief,[2] L. Largeau,[1] M. Portail,[4] B. Fain,[1] and F. Sirotti[3]

[1]*Laboratoire de Photonique et de Nanostructures (LPN), CNRS, Route de Nozay, 91460 Marcoussis, France*

[2]*Institut des NanoSciences de Paris (INSP), Université Pierre et Marie Curie-Paris 6–CNRS, UMR 7588 Campus Boucicaut, 140 rue de Lourmel, 75015 Paris, France*

[3]*Synchrotron-SOLEIL, Saint-Aubin, BP 48, F91192 Gif sur Yvette Cedex, France*

[4]*CNRS-CRHEA, Rue Bernard Gregory, 06560 Valbonne, France*

(Received 23 June 2010; revised manuscript received 26 July 2010; published 24 September 2010)

Structural and electronic properties of epitaxial graphene on 3C-SiC(111) pseudosubstrate epilayers on silicon was investigated in detail by scanning tunneling microscopy (STM), low-energy electron diffraction (LEED), scanning transmission electron microscopy (STEM), and synchrotron angle-resolved photoemission spectroscopy (ARPES). The graphitization process has been observed by distinct features in the atomically resolved STM images and abrupt interface with the number of stacked-graphene layer has been revealed in STEM image. Two different types of carbon atom networks, honeycomb and one sublattice, were atomically resolved by STM. Electronic properties and band structures of the epitaxial graphene are examined with angle-resolved photoemission spectroscopy, showing linear band dispersion K point of the Brillouin zone, with Dirac point about 500 meV below the Fermi level (E_F). These findings are of relevance for various potential applications based on graphene-SiC/Si(111) structures.

DOI: 10.1103/PhysRevB.82.125445 PACS number(s): 68.65.Pq, 61.48.Gh, 61.05.jh

I. INTRODUCTION

The recent success of graphene transistor operation in the gigahertz range has highlighted the potential of this material for high-speed electronic applications.[1] However the realization of graphene technologies at commercial scales needs large area and homogeneous graphene layers production, as well as the ability to rapidly characterize their structural, electronic, and transport properties. A number of fundamental studies of graphene have been carried out recently mainly based on the micromechanical cleavage of single-layer flakes from graphite,[2] anodic bonding,[3] chemical vapor deposition on catalytic films,[4] or Si sublimation from bulk silicon carbide (SiC) substrates.[5] The last technique currently appears to hold the most promise for large-area graphene production by simply heating substrates exhibiting a tendency toward graphitization. Indeed, the preferential sublimation of Si atoms from a SiC substrate[1,6] offers an appealing way to grow few layer graphene on wafer-size substrates and already shows tremendous potential for high-frequency device technologies.

Prior investigations of 6H- and 4H-SiC(0001) surfaces showed that graphene films can be grown on these substrates by sublimating Si from the SiC substrates after heating process above 1300 °C in ultrahigh vacuum (UHV) or in inert argon atmosphere.[5,7] An important aspect of the preparation of epitaxial graphene is the layer homogeneity and the ability to obtain large-area graphene. In this context an accurate control and understanding of the structure and the electronic properties are of prime importance. The most used methods are scanning tunneling microscopy and spectroscopy (STM/STS),[8–12] low-energy electron microscopy (LEEM),[13,14] x-ray photoelectron spectroscopy (XPS),[15–17] angle-resolved photoemission spectroscopy (ARPES),[18,19] Raman spectroscopy, and magnetotransport.[5] Obtaining homogeneous large-area graphene layer remains hard to acheive. The challenge is to grow graphene on a large-diameter substrate, a process with high industrial impact for future mass production. To address this issue, the *heteroepitaxy* of relaxed cubic polytype (3C-SiC) on silicon wafers (pseudosubstrate) was proposed.[20–22] The graphene layers can be directly patterned by standard Si-electronic lithographic processes. Recently, we have shown using XPS and Raman spectroscopy that high structural quality epitaxial graphene on 600 nm 3C-SiC(111) pseudosubstrate has been obtained.[22]

In this paper, we present recent results concerning the structural and electronic properties of epitaxial graphene layers grown on pseudosubstrate 3C-SiC(111) by solid-state graphitization. These results have been obtained using a large combination of experimental methods. Our diffraction and STM measurements clearly show that graphene layers are atomically flat. Bias-dependent STM images recorded are consistent with the Bernal *ABAB* stacking, as found in the most common form of graphite. ARPES measurements confirm that the electronic dispersion is linear in the vicinity of the Dirac cone. These studies highlight the importance of underlying graphene/3C-SiC(111) layer in determining the electronic properties of epitaxial graphene.

II. EXPERIMENTAL DETAILS

The 3C-SiC epilayers on *n*-doped silicon were deposited using classical two steps chemical-vapor deposition process using silane and propane as precursors, performed within a resistively heated hot wall reactor.[23] In order to prevent stress induced the formation of cracks at the surface, the film thickness was limited to 600 nm. This value is measured by scanning transmission electron microscopy (STEM) and well below the critical thickness reported for growth performed on

axis films.[24] A fine tuning of the experimental parameters (carbon content during the nucleation step and carbon/silicon ratio during the growth) is required to achieve well coalesced 3C-SiC epilayers.[23] The surface morphology of the 3C-Si(111) is characterized by the presence of threefold symmetric terraces distributed over the surface (root-mean-square roughness as about 0.5 nm). The triangular terraces is related to the anisotropic in-plane growth rates for fcc(111) faces which lead to observe facets perpendicular to the lowest growth rates.[21]

Graphene on unpolished 3C-SiC(111) pseudosubstrate were prepared in UHV ($P=2\times10^{-10}$ Torr) by electron-bombardment heating at 1300 °C.[22] The samples were introduced into the UHV growth chamber, followed by *in situ* degassing at 650° ± C for 1 h. The substrates were then annealed under a Si flux (1 ML/min) at 700 °C in order to remove the native oxide. All of the samples were examined by low-energy electron diffraction (LEED) during the whole annealing process without Si flux. The epitaxial graphene samples were cooled down then to room temperature and transferred *ex situ* from the growth chamber to STM and ARPES chambers. Once introduced in the analysis chambers, the samples are degassed for 1 h at a temperature of 600 °C prior to the STM and ARPES measurements.

STM experiments were carried out using an UHV atomic force microscopy-STM Omicron ($<5\times10^{-11}$ Torr) at room temperature. Band-structure $[E(k_{\|})]$ maps were obtained at room temperature by collecting angle-resolved valance-band spectra. The ARPES experiments were performed in UHV conditions at TEMPO beamline at the SOLEIL Synchrotron Facility (France). The photon energy was set to $h\nu=50$ eV, providing high surface sensitivity, high photon intensity, and maximizing the valance-band cross section. The raw data comprised photoelectron angular distributions beyond the first Brillouin zone for energies from −22 eV to +2 eV relative to E_F in increments of 0.05 eV. Projections along high-symmetry directions in reciprocal space were used to generate band-structure maps along those directions. The valance-band spectra have been recorded using a R2000 Scienta anylser with an overall energy resolution of 50 meV and an angular resolution below 0.1°. The photon energy and the sample orientation were set in order to explore the *k*-space region around the K point along the ΓK direction.

For STEM measurements, a dedicated 3C-SiC (111) sample was mechanically thinned prior to the preparation of the graphene layers. Following this process, the sample could be easily cleaved after the growth of the graphene without inducing any damage of the graphene layers. The cleaved bars were then stuck, thinned mechanically and Ar^+ ion milled.

III. RESULTS AND DISCUSSION

LEED patterns have been collected for graphene layer grown on the 3C-SiC(111) surface as shown in Fig. 1 in order to follow up the structural changes (surface reconstruction) induced by the annealing temperature without Si flux. Immediately after introduction into UHV and before any outgasing, the samples exhibited a clear (1×1) LEED pattern,

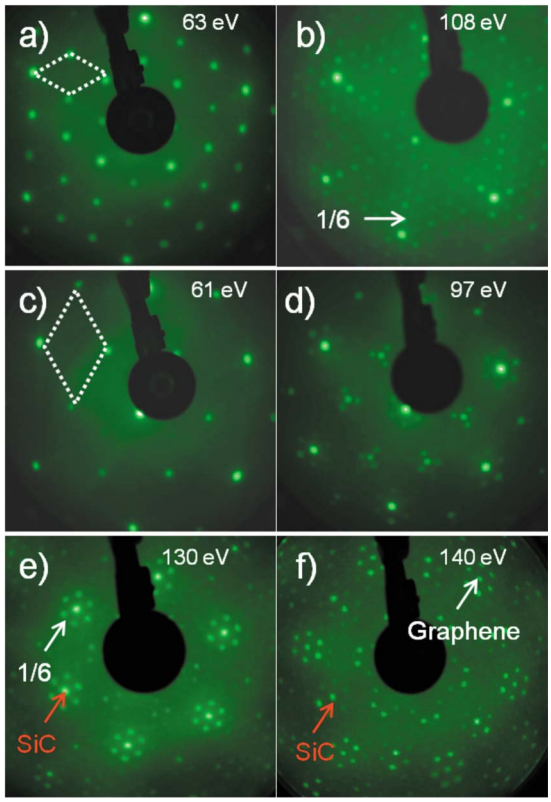

FIG. 1. (Color online) LEED patterns of differently reconstructed of 3C-SiC(111) obtained increasing the annealing at different temperature without Si flux (a) (3×3) phase after annealed at 800 °C; (b) (6×6) phase after annealed at 900 °C; (c) $(\sqrt{3}\times\sqrt{3})R30°$ phase after annealed at 1050 °C; (d) $(\sqrt{3}\times\sqrt{3})R30°+(6\sqrt{3}\times6\sqrt{3})R30°$ after annealed at 1100 °C; (e) $(6\sqrt{3}\times6\sqrt{3})R30°$ after annealed at 1200 °C; and (f) epitaxial graphene layer after annealed at 1250 °C.

which belongs to the threefold and sixfold rotational symmetries for the cubic substrates. Figure 1(a) shows the LEED pattern after the sample was annealed at 800 °C under Si flux (0.5 ML/min) for 15 min. Sharp spots with a (3×3) periodicity are clearly observed, indicating the formation of a Si-rich surface. The sample surface evidences a variety of LEED reconstruction as a function of the annealing temperature without Si flux, process that we used in order to grow graphene film by desorbing excessive Si surface atoms.[25] An annealing process at 900 °C for 5 min leads to a (6×6) Si terminated [Fig. 1(b)]. The observed structural evolution must be related to thermally induced Si desorption, this would imply that the (6×6) surface is a Si-rich surface. A similar surface termination and structure has been briefly noticed by Ong and Tok[26] during the annealing of a 6H-SiC(0001) surface without being further and deeply interpreted. At 1050 °C, only 1/3 monolayer of Si atoms remained at the surface, showing the typical $(\sqrt{3}\times\sqrt{3})R30°$ reconstruction on 3C-SiC(111) [Fig. 1(c)]. Further annealing at 1100 °C leaded to a mixture of a $(\sqrt{3}\times\sqrt{3})R30°+(6\sqrt{3}\times6\sqrt{3})R30°$ reconstruction phases, as shown in Fig. 1(d). However, still no single-phase graphene layer was formed at this temperature. At 1200 °C the $\sqrt{3}$ reconstruction disappears and only the $(6\sqrt{3}\times6\sqrt{3})R30°$ su-

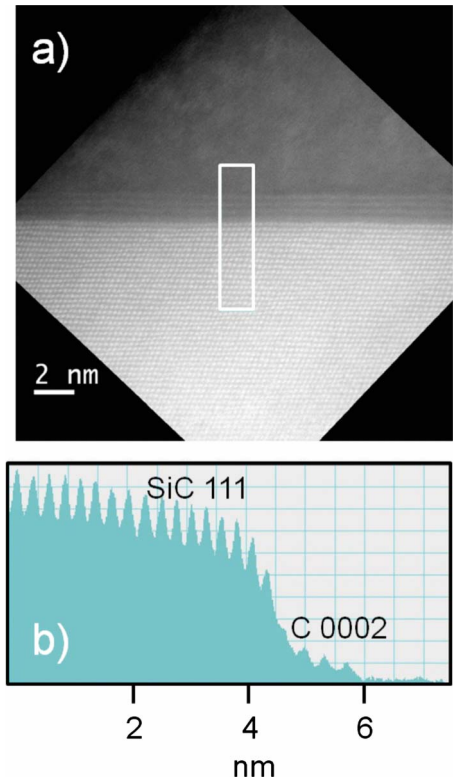

FIG. 2. (Color online) (a) High-resolution STEM image obtained of the sample annealed at 1300 °C and (b) line profile of STEM image show the epitaxial of three layer graphene.

perstructure was observed [Fig. 1(e)]. Hence, we increased the annealing temperature up to 1250 °C to track the graphene layer. As shown in Fig. 1(f), a single phase of graphene layer is formed as deduced from the very well ordered $(6\sqrt{3}\times 6\sqrt{3})R30°$ LEED pattern that correspond to a Carbon-rich termination. The smallest hexagons around the integer spots are due to double diffraction and is the result of a $(6\sqrt{3}\times 6\sqrt{3})R30°$ reconstruction of the interfacial layer. These LEED findings well matches previously reported result.[15,27] The changes in LEED altogether reveal the onset of real epitaxial graphene layers on SiC pseudosubstrate, which proceeds following the same manner as during the epitaxy of graphene on 6H-SiC(0001) bulk.

To further investigate the structural properties, cross-sectional STEM and STM experiments were performed on three layers epitaxial graphene (after annealing at 1300 °C for 10 mn). Figure 2 is observed in the high angle annular dark field (HAADF) STEM mode using a Cs-probe aberration corrected JEOL 2200 FS STEM [Fig. 2(a)]. Although HAADF technique is commonly used to observe semiconductors because of its high sensitivity to composition variation combined with an atomic resolution, observation of graphene is much harder since carbon layer can be damaged by the electron beam. In the STEM image the 3C-SiC lattice planes are straight, sharp, parallel to the surface and equidistant. The line profile in Fig. 2(b) of the topmost 18 SiC planes confirms that their spacing is indeed constant (2.5 Å) and attests to the abruptness of the graphene/3C-SiC(111) interface under the growth conditions reported here: no detectable sign of interdiffusion and intermixing has been observed. The graphene layer shows different contrast from the SiC and appears slightly wavy. We measured a distance of 3.35 ± 0.15 Å between each graphene layer, this value is very close to the bulk interplanar distance (3.376 Å). The average spacing between the SiC surface plane and the first carbon layer is measured to be 2.9 Å, which is in good agreement with the distance between the interface layer and substrate of graphene layer on 6H-SiC(0001).[28] This value is considerably larger than Si-C bond length in SiC crystal (1.89 Å), which are closer than that in bulk graphite.[29] The difference between experimentally and theory values can be attributed to strain which builds up during the cool down procedure. However, if we assume that the mismatch between the $(6\sqrt{3}\times 6\sqrt{3})R30°$ reconstructed surface and 3C-SiC(111) is completely relaxed at the growth temperature, a residual *compressive* strain arises during sample cooling to room temperature because of the large difference in the coefficients of linear thermal expansion between monolayer carbon and SiC. Obviously the carbon layer can change its volume only by unaxial expansion in the growth direction $[111]_{SiC}$, likely due to out-of-plane surface relaxation. This result will be explained the complex structure of the interface structure. Recently, Raman measurement points to a compressive strain in plane of the epitaxial graphene layer.[17,22] Grazing incidence x-ray diffraction is crucial in order to determine the atomic structure of this reconstructed surface.

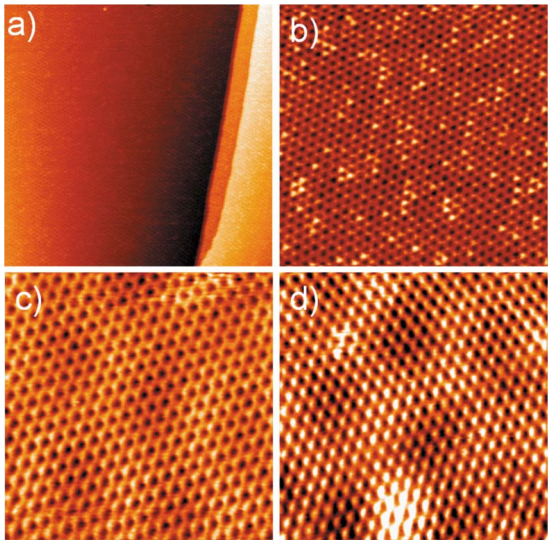

FIG. 3. (Color online) STM micrographs of graphene/3C-SiC(111) epilayers: (a) STM images (150×150 nm^2) (−2 V, 0.2 nA), (b) STM images (50×50 nm^2) (−2 V, 0.2 nA), (c) Honeycomb type structures (5×5 nm^2) (−45 mV, 0.2 nA), and (d) triangular type structures (5×5 nm^2) (−25 mV, 0.2 nA) of the surface of graphene/3C-SiC(111).

In order to assess to the continuity of the graphene layer, we performed STM measurements at room temperature. Figure 3 shows STM image of the sample before STEM study. This image shows that the terraces are fully covered by atomic flat graphene presenting a $(6\sqrt{3}\times 6\sqrt{3})R30°$ surface reconstruction. Each terrace is completely covered by a single domain of graphene and the domains on different ter-

races are continuous and oriented in the same direction. Atomically flat terraces separated by monolayer steps edges are clearly resolved. The step edges are parallel to the ⟨110⟩ directions of the 3C-SiC(111) substrate [Fig. 3(a)]. Figure 3(b) shows a higher resolution image at higher bias voltage (−2 V), illustrating clearly the hexagonal moiré pattern observed in LEED. On the other hand, the surface appears to be flat and homogeneous even in the large-scale images (100×100 nm^2). In real space the average distance between the neighboring moiré spots measured in both directions is 1.8 nm, which correspond to six times of SiC lattice [(6×6) reconstruction]. This structure is attributed to a C-rich $(6\sqrt{3}\times6\sqrt{3})R30°$ reconstruction of the SiC buffer layer below the graphene, in agreement with previous reports.[10–15] On 6H-SiC(0001) substrate, STM images have shown the presence of the $(6\sqrt{3}\times6\sqrt{3})R30°$ structure. It was explained as a moiré patterns caused by a carbon layer sitting on top of the SiC surface.[30–32] This model suggesting that this reconstruction corresponds to a monolayer of carbon on top of a (1×1)-6H-SiC(0001) surface.[4] We conclude that the $(6\sqrt{3}\times6\sqrt{3})R30°$ structure can be represented with a moiré pattern comprising of a multiple diffraction between an unreconstructed (1×1) SiC substrate and the graphene overlayer rotated by 30° with respect to the substrate.[9,10]

Furthur, a honeycomb lattice superposed on the $(6\sqrt{3}\times6\sqrt{3})R30°$ structure can be observed also when the sample bias is set to a low voltage. The periodicity of this structure is equal to 2.5 ± 0.1 Å which is in good agreement with the (1×1) graphene lattice.[10,30] Figures 3(c) and 3(d) show two STM images from a layer terrace. The atomically resolved STM images are recorded from the same area of the graphene sample, but the sample bias was switched between two values, while keeping all the other scan parameters fixed. This procedure allows achieving high sensitivity to spatial variations in the energy dependence of the local density of states (DOS) for the two sublattices in graphene. At an even higher tunneling bias of −45 mV the image shows a honeycomb structure similar to that observed for single-layer graphene, where both sublattices are imaged at almost the same intensity [Fig. 3(c)]. A graphene lattice is composed by *A* and *B* sublattices, this asymmetry in the surface atom electronic environment results in a threefold symmetry (six-for-three) pattern in which three bright or dark features can be observed for each set of six carbon atoms. At a sample bias of −25 mV, the graphene lattice appears triangular indicating that only one of the two graphene sublattices is imaged due to Bernal stacking of bilayer graphene [Fig. 3(d)]. Similar images have been observed in STM studies of bulk graphite and multilayer graphene surfaces. This layer epitaxial graphene is shown to be Bernal stacked as it is evidenced by bias-dependent topographic imaging.[15,33]

To further explore the electronic properties of monolayer epitaxial graphene, we have performed synchrotron-based ARPES measurements of graphene on 3C-SiC(111) at room temperature. The C 1*s* core-level spectrum measured with a photon energy of 340 eV is presented in Fig. 4(a). The characteristic signals of the graphene monolayer (G), SiC substrate and $(6\sqrt{3}\times6\sqrt{3})R30°$ interface layer in accordance with C 1*s* spectrum of few epitaxial monolayer graphene on 6H-SiC(0001) substrate.[16] This thickness (monolayer

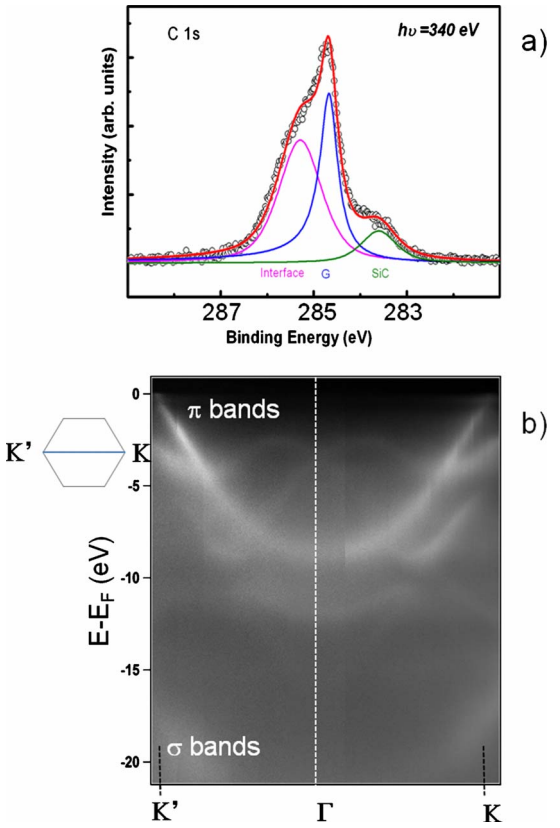

FIG. 4. (Color online) Electronic structure of graphene/3C-SiC(111) near the K point obtained by ARPES (a) C 1*s* core-level spectrum for monolayer graphene; decomposition with bulk and two surfaces components identified by SiC, G, and interface, respectively, (b) Band-structure mapping by ARPES of a graphene monolayer grown on the 3C-SiC(111). Inset, photoemission image measured in the k_x direction.

graphene) measurement is corroborated by the attenuation observed in the Si 2*p* XPS and Raman spectroscopy measurement.[22,34] To demonstrate the crystallinity of a monolayer graphene we have performed an ARPES experiment to obtain direct information of the electronic band structure. The map of the angular-resolved photoemission spectra of the valence band are shown in Fig. 4(b) for a monolayer graphene annealed at 1250 °C. The data were taken along the K′ΓK direction as shown in the sketch of Fig. 4(b). The smaller feature near Γ point and around −2.5 eV binding energy can be attributed to the $(6\sqrt{3}\times6\sqrt{3})R30°$ reconstruction surface. These findings are in agreement with a recent APRES study of monalyer graphene on 6H-SiC(0001).[15]

The graphene band structure dominated by σ and π bands is clearly discernable [Fig. 4(b)]. The π band of the outer layer crosses the Fermi level E_F and shows a linear dispersion at K and recovers the signature of massless Dirac fermions characteristic of isolated monolayer graphene. There is an excellent overall matching over the entire Brillouin zone if we assume an electron-doped epitaxial graphene layer whose Dirac point lays 500 meV below E_F. These measurements confirm the conclusions drawn on the basis of the line-shape analysis of the double-resonant two-dimensional

Raman line[22] that the outer sheet of epitaxial graphene layer on SiC(111) adopts essentially the electronic structure and signature of a monolayer graphene.

Hence, the electron (or hole) doping is believed to be associated with surface charges at the interface and the energy shift of the π band is influenced by the number of layers.[15] Using the linear dispersion of the density-of-states (DOS) near the Dirac point, the charge carrier concentration (electron or hole) of doped monolayer graphene can be estimated as: $|n|=(E_F-E_D)^2/(\pi)(\hbar v_F)^2$, where $\hbar$ is the Planck's constant, v_F the Fermi velocity ($v_F=1.1\times10^6$ m/s), and E_D the energy position of the Dirac point. The resulting electron density is about $n\sim1.8\times10^{13}$ cm^{-2} for our epitaxial graphene on 3C-SiC(111) pseudosubstrate. Note that, like the graphene grown on 6H-SiC(0001),[20,23,24] the Dirac point (E_D) is shifted below the Fermi level (E_F) due to electron doping ($n\approx4.1\times10^{13}$ cm^{-2}) induced by the substrate. This clear conductor behavior of the layer is in agreement with previous experiments for graphene on 6H-SiC(0001) (Refs. 8–10) and provides evidence for the feasibility of synthesizing homogeneous epitaxial graphene films over large area. Further investigations are currently carried out using quantitative low-temperature STM/STS.

We now discuss briefly why the graphene surface is obtained after the cycle of SiC pseudosubstrate sublimation. First of all, we want outline that the successive surface reconstructions steps observed during the thermal treatment of the 3C-SiC(111)/Si(111) are similar to those observed on Si terminated 6H or 4H-SiC(0001) substrates.[9] Moreover, observation of identical surface reconstruction processes both on a zinc blende and a wurtzite material shows that the intrinsic piezoelectric polarization, which is expected to occur only within wurtzite substrates, is negligible in the surface rearrangement mechanism. In addition, STM images shows a (6×6) reconstruction with respect to the unreconstructed surface 3C-SiC(111). With low bias, a clear honeycomb lattice can be put in evidence, superposed on (6×6) structure (Fig. 3). This observation indicates that the interaction of graphene layer with the SiC substrate is mediated by the interfacial $(6\sqrt{3}\times6\sqrt{3})R30°$ layer arranged in a honeycomb lattice. This strong bond is responsible for the orientation of the reconstruction layer, which shows a rotation angle of 30° with respect to the substrate and gives rise to the (6×6) reconstruction. As a consequence π states of the buffer layer are removed from the vicinity of the Fermi level, and STM images do not reveal the graphene atomic lattice. Annealing to higher temperature results in further desorption of Si, which promotes the formation of a second carbon layer, and deprives the original (topmost) carbon atoms of their covalent bonds to Si atoms, inducing the sp^2 bonding configuration.[29] ARPES experiments indicate that the first and the following graphene layer on top of the interface have a graphene electronic structure and, therefore, interact only weakly by van der Waals forces with the interface layer (Fig. 4). These findings are in agreement with a recent photoemission study, which concludes from valence-band and core-level spectra that the interaction between the first graphene layer grown on 6H-SiC and the substrate is small. In particular, they could observe the π band close to E_F for monolayer graphene coverage.[15] Varchon *et al.*[30] have performed density-functional theory calculations on 4H-SiC(0001) and 6H-SiC, deducing a considerable covalent orbital coupling of first all-carbon layer to the substrate; it is only the second carbon layer that exhibits true graphene properties. Finally, our result shows that 3C-SiC/Si(111) pseudosubstrate can be used in the same way as more commonly 6H or 4H-SiC(0001) substrates.

IV. CONCLUSION

In summary, we have presented detailed measurements of structure and electronic properties of epitaxial graphene layers on 3C-SiC(111) pseudosubstrate obtained via large combination of experimental methods. The average spacing between the SiC and interface layer is measured to be 2.9 Å, which is considerably larger than Si-C bond length in SiC crystal (1.89 Å), which are closer than that in bulk graphite. Bias-dependent STM images recorded are consistent with the Bernal *ABAB* stacking. Electronic property of graphene layer was confirmed by the conical band structure of the π bands around the K point of the graphene Brillouin zone by ARPES. The observed Dirac cones definitively demonstrate that the graphene monolayer can be considered as electronically ideal isolated graphene sheets.

ACKNOWLEDGMENTS

The authors thank T. Chassagne and M. Zielinski from Novasic for fruitful discussion. Thank Damjan Krizmancic of TASC Laboratory in Trieste for software developments in data analysis and data acquisition procedures. A.O. thanks B. Etienne and L. Travers for fruitful and stimulating discussions.

[1] Y. M. Lin, C. Dimitrakopoulos, K. A. Jenkins, D. B. Farmer, H.-Y. Chiu, A. Grill, and Ph. Avouris, Science **327**, 662 (2010).

[2] K. S. Novoselov, A. K. Geim, S. V. Morozov, D. Jiang, Y. Zhang, S. V. Dubonos, I. V. Grigorieva, and A. A. Firsov, Science **306**, 666 (2004).

[3] A. Shukla, R. Kumar, J. Mazher, and A. Balan, Solid State Commun. **149**, 718 (2009); A. Balan *et al.*, J. Phys. D: Appl. Phys. **43**, 374013 (2010).

[4] K. S. Kim, Y. Zhao, H. Jang, S. Y. Lee, J. M. Kim, K. S. Kim, J.-H. Ahn, P. Kim, J. Y. Choi, and B. H. Hong, Nature (London) **457**, 706 (2009).

[5] C. Berger, Z. M. Song, X. B. Li, X. S. Wu, N. Brown, C. Naud, D. Mayo, T. B. Li, J. Hass, A. N. Marchenkov, E. H. Conrad, P. N. First, and W. A. de Heer, Science **312**, 1191 (2006).

[6] J. Kedzierski, P. L. Hsu, P. Healey, P. W. Wyatt, C. L. Keast, M. Sprinkle, C. Berger, and W. A. de Heer, IEEE Trans. Electron

Devices **55**, 2078 (2008).
[7] K. V. Emtsev, A. Bostwick, K. Horn, J. Jobst, G. L. Kellogg, L. Ley, J. L. McChesney, T. Ohta, S. A. Reshanov, J. Röhrl, E. Rotenberg, A. K. Schmid, D. Waldmann, H. B. Weber, and T. Seyller, Nature Mater. **8**, 203 (2009).
[8] W. V. Brar, Y. Zhang, Y. Yayon, T. Ohta, J. L. McChesney, A. Bostwick, E. Rotenberg, K. Horn, and M. F. Crommie, Appl. Phys. Lett. **91**, 122102 (2007).
[9] P. Lauffer, K. V. Emtsev, R. Graupner, T. Seyller, L. Ley, S. A. Reshanov, and H. B. Weber, Phys. Rev. B **77**, 155426 (2008).
[10] P. Mallet, F. Varchon, C. Naud, L. Magaud, C. Berger, and J. Y. Veuillen, Phys. Rev. B **76**, 041403(R) (2007).
[11] C. Riedl, A. A. Zakharov, and U. Starke, Appl. Phys. Lett. **93**, 033106 (2008).
[12] L. Vitali, C. Riedl, R. Ohmann, I. Brihuega, U. Starke, and K. Kern, Surf. Sci. **602**, L127 (2008).
[13] T. Ohta, F. El Gabaly, A. Bostwick, J. L. McChesney, K. V. Emtsev, A. K. Schmid, T. Seyller, K. Horn, and E. Rotenberg, New J. Phys. **10**, 023034 (2008).
[14] H. Hibino, H. Kageshima, F. Maeda, M. Nagase, Y. Kobayashi, and H. Yamaguchi, Phys. Rev. B **77**, 075413 (2008).
[15] K. V. Emtsev, F. Speck, T. Seyller, L. Ley, and J. D. Riley, Phys. Rev. B **77**, 155303 (2008).
[16] J. Penuelas, A. Ouerghi, D. Lucot, C. David, J. Gierack, H. Estrade-Szwarckopf, and C. Andreazza-Vignolle, Phys. Rev. B **79**, 033408 (2009).
[17] Z. H. Ni, W. Chen, X. F. Fan, J. L. Kuo, T. Yu, A. T. S. Wee, and Z. X. Shen, Phys. Rev. B **77**, 115416 (2008).
[18] T. Ohta, A. Bostwick, J. L. McChesney, T. Seyller, K. Horn, and E. Rotenberg, Phys. Rev. Lett. **98**, 206802 (2007).
[19] S. Y. Zhou, G.-H. Gweon, A. V. Fedorov, P. N. First, W. A. de Heer, D.-H. Lee, F. Guinea, A. H. Castro Neto, and A. Lanzara, Nature Mater. **6**, 770 (2007).
[20] V. Y. Aristov, G. Urbanik, K. Kummer, D. V. Vyalikh, O. V. Molodtsova, A. B. Preobrajenski, A. A. Zakharov, C. Hess, T. Hänke, B. Büchner, I. Vobornik, J. Fujii, G. Panaccione, Y. A. Ossipyan, and M. Knupfer, Nano Lett. **10**, 992 (2010).
[21] A. Ouerghi, M. Portail, A. Kahouli, L. Travers, T. Chassagne, and M. Zielinski, Mater. Sci. Forum **645-648**, 585 (2010).
[22] A. Ouerghi, A. Kahouli, D. Lucot, M. Portail, L. Travers, J. Gierak, J. Penuelas, P. Jegou, A. Shukla, T. Chassagne, and M. Zielinski, Appl. Phys. Lett. **96**, 191910 (2010).
[23] M. Portail, M. Zielinski, T. Chassagne, S. Roy, and M. Nemoz, J. Appl. Phys. **105**, 083505 (2009).
[24] J. Nishizawa and M. Kimura, J. Cryst. Growth **74**, 331 (1986).
[25] J. Schardt, J. Bernhardt, U. Starke, and K. Heinz, Phys. Rev. B **62**, 10335 (2000).
[26] W. J. Ong and E. S. Tok, Phys. Rev. B **73**, 045330 (2006).
[27] U. Starke and C. Riedl, J. Phys.: Condens. Matter **21**, 134016 (2009).
[28] W. Norimatsu and M. Kusunoki, Chem. Phys. Lett. **468**, 52 (2009).
[29] J. Borysiuk, R. Bożek, W. Strupiński, A. Wysmołek, K. Grodecki, R. Stępniewski, and J. M. Baranowski, J. Appl. Phys. **105**, 023503 (2009).
[30] F. Varchon, R. Feng, J. Hass, X. Li, B. N. Nguyen, C. Naud, P. Mallet, J.-Y. Veuillen, C. Berger, E. H. Conrad, and L. Magaud, Phys. Rev. Lett. **99**, 126805 (2007).
[31] Y. Marumoto, T. Tsukamoto, M. Hirai, M. Kusaka, M. Iwami, T. Ozawa, T. Nagamura, and T. Nakata, Jpn. J. Appl. Phys., Part 1 **34**, 3351 (1995).
[32] C. S. Chang and I. S. T. Tsong, Surf. Sci. **256**, 354 (1991).
[33] G. M. Rutter, J. N. Crain, N. P. Guisinger, T. Li, P. N. First, and J. A. Stroscio, Science **317**, 219 (2007).
[34] C. Virojanadara, M. Syväjarvi, R. Yakimova, L. I. Johansson, A. A. Zakharov, and T. Balasubramanian, Phys. Rev. B **78**, 245403 (2008).